Bidirectional reflectance of laboratory cometary analogues to interpret the spectrophotometric properties of the nucleus of comet 67P/Churyumov-Gerasimenko

Bernhard Jost[a,*], Antoine Pommerol[a], Olivier Poch[b], Yann Brouet[a], Sonia Fornasier[c,d], Nathalie Carrasco[e,f], Cyril Szopa[e,f], Nicolas Thomas[a]

[a] *Physikalisches Institut, Universität Bern, Sidlerstrasse 5, CH-3012 Bern, Switzerland*
[b] *NCCR PlanetS, University of Bern, Sidlerstrasse, 5, 3012 Bern, Switzerland*
[c] *LESIA, Observatoire de Paris, CNRS, UPMC Univ Paris 06, Univ. Paris-Diderot, 5 place J. Janssen, 92195 Meudon Pricipal Cedex, France*
[d] *Univ Paris Diderot, Sorbonne Paris Cit, 4 rue Elsa Morante, 75205 Paris Cedex 13, France*
[e] *UniversitVersailles St-Quentin ; Sorbonne Universitś, UPMC Univ. Paris 06 ; CNRS/INSU, LATMOS-IPSL, 11 Boulevard dAlembert, 78280 Guyancourt, France*
[f] *Institut Universitaire de France, 103 Bvd St-Michel, 75005 Paris, France*

Abstract

In this work we provide measurements of the bidirectional reflectance in the VIS-NIR spectral range for a selection of laboratory samples to deduce parameters such as their visible spectrum, phase curve, hemispheric albedo and phase reddening. The aim is to simulate the reflectance of the comet nucleus in order to aid the interpretation of data from the surface of comet 67P/Churyumov-Gerasimenko (67P) acquired by the Rosetta OSIRIS imaging system. We produced a broad variety of well characterised and reproducible samples containing water ice, carbonaceous compounds and complex organic molecules. We were able to reproduce the individual global spectrophotometric parameters (albedo, spectrum, phase reddening, phase curve) of 67P by using mixtures of activated charcoal, tholins and water ice. However, no mixture was able to fit all parameters simultaneously. The samples with highest porosities best match the phase curve of 67P. Spectral considerations from our experiments show that the parti-

*Corresponding author
Email address: bernhard.jost@space.unibe.ch (Bernhard Jost)

source: https://doi.org/10.7892/boris.106337 | downloaded: 25.4.2024

cle size of the darkening agent on the cometary surface should have a lower limit of a few hundred nanometres to several micrometres and cannot be dominated by particles in the range of some tens of nanometres. Furthermore, our findings indicate that the bright ice patches observed by OSIRIS and VIRTIS should be relatively dust free at small scale.

Keywords: Photometry, water ice, organics, comets

1. Introduction

After its ten-year interplanetary journey, ESAs Rosetta spacecraft arrived at comet 67P/Churyumov-Gerasimenko (67P) in August 2014. Since then the nucleus has been scrutinised and mapped regularly by the Optical, Spectroscopic, and Infrared Remote Imaging System (OSIRIS) (Keller et al., 2007) consisting of a Narrow Angle Camera (NAC) and a Wide Angle Camera (WAC). First imaging and spectroscopy results from the OSIRIS and VIRTIS[1] instruments showed unexpected surface morphology and diversity (Sierks et al., 2015; Thomas et al., 2015; Capaccioni et al., 2015).

A detailed analysis of OSIRIS data of the spectrophotometric properties of 67Ps nucleus was carried out by Fornasier et al. (2015), finding a strong opposition peak on the phase function, a red spectral behaviour in the UV to NIR spectral range without absorption bands and a strong phase reddening. According to the spectral slopes they define three groups (blue, moderately red, and red) of terrains across the nucleus. The blue terrains mainly lie in the neck region, while the two lobes are more red.

To link these spectrophotometric properties to physical surface characteristics such as chemical composition, grain sizes, porosity and texture, a profound knowledge of analogues is vital. Since the resolution of OSIRIS is limited to the

[1] Visible and Infrared Thermal Imaging Spectrometer, Coradini et al., 2007

centimetres to metres range, depending on the spacecraft-nucleus distance, it will never be possible to draw any direct conclusion about surface properties on the millimetre- or submillimetre- scale from this dataset. Other instruments on Rosetta and Philae can however provide information on the physical and chemical properties of the surface at smaller scales, either directly (CIVA and ROLIS images at resolutions down to 0.8 mm/px; Bibring et al., 2007; Mottola et al., 2007; Schröder et al., 2017) or indirectly, from the inversion of remote-sensing data (MIRO, Gulkis et al., 2007; VIRTIS, Coradini et al., 2007).

A common finding of Rosetta is the absence of extended surface regions of exposed water ice, in general agreement with previous observations of cometary nuclei such as 9P/Tempel 1 (Sunshine et al., 2006) or 103P/Hartley 2 (A'Hearn et al., 2011; Protopapa et al., 2014). A notable exception are two bright 1500 square metre wide patches observed in the Anhur/Bes regions (Fornasier et al., 2016). The global surface is mainly covered by carbon-bearing, dehydrated, refractory and organic-rich material (Capaccioni et al., 2015). Nevertheless OSIRIS's high-resolution images revealed over one hundred metre-sized bright spots dispersed over the comets surface, mainly in low insolation areas, that were hypothesized to be ice-rich features (Pommerol et al., 2015b; Deshapriya et al., 2016). The presence of water ice on two large debris falls in the Imhotep region has indeed been confirmed by the Visible Infrared and Thermal Imaging Spectrometer (VIRTIS), with a spatial resolution of $15 - 30$ m (Filacchione et al., 2016). Spectral fitting and inversion indicates crystalline pure water ice grains with a bimodal grain size distribution with peaks at $33 - 72$ µm and $1.4 - 2.6$ mm. The occurrence of millimetre-sized particles can be explained by growth by vapour diffusion in ice-rich layers or by sintering. This particle size is significantly larger than the 1 µm grains (and agglomerates of them) that were reported in the coma of comet 103P/ Hartley 2 (Sunshine et al., 2011). Further comparisons of the OSIRIS and VIRTIS datasets have led to the conclusion that most of the bright features observed by OSIRIS were indeed exposures of dirty water ice (Barucci et al., 2016) of indeterminate the grain size.

In addition to chemical composition the morphological properties of ejected non-volatile grains were analysed by the optical microscope of the Cometary Secondary Ion Mass Analyzer (COSIMA, Kissel et al., 2007) with a spatial resolution of 14 µm. Larger grains exceeding 50 µm are fluffy and most likely agglomerates (Schulz et al., 2015). Hilchenbach et al. (2016) report on particle sizes ranging from 15 µm to 225 µm with a differential size distribution fitted with a power law exponent of -3.1, meaning a large number of small particles.

Measurements by the Grain Impact Analyzer and Dust Accumulator (GIADA, Colangeli et al., 2007) revealed porous aggregates (0.2 to 2.5 mm) of submicron particles (Della Corte et al., 2015). Fulle et al. (2015) report on a second family of compact particles in the size range of 0.03 to 1 mm. Nevertheless post-landing images at highest resolution taken by ROLIS did not reveal any particles (Schröder et al., 2017), suggesting a surface consisting of small particles without agglomerates formation at this site. Preliminary analyses of the Micro-Imaging Dust Analysis System (MIDAS, Riedler et al., 2007) reveal only very few small (sub-micron) particles, but several particles much larger than expected (Bentley et al., 2015). It is not clear whether these results represent the dust composition on the surface of the comet or if they are biased in terms of chemical composition, size and shapes as all data is collected in the coma of 67P.

To better understand and interpret the observational data and findings it is crucial to comprehend the physical processes involved. A useful approach is to conduct representative laboratory simulations in order to quantify these processes and provide a starting point for numerical models. Until now only a few laboratory studies investigated the optical properties and surface evolution of cometary analog materials using ice/non-volatile mixtures. The most extensive and comprehensive campaign was the KOSI (KOmeten-Simulations) experiments performed at the DLR space simulator in Köln from 1987 to 1993 (Gruen et al., 1991; Gruen et al., 1993; Seiferlin et al., 1995). A brief review can

be found in Sears et al. (1999). These experiments focuses on the surface evolution and sublimation processes under simulated space conditions pursuant to findings of ESA's Giotto mission to comet 1P/Halley. Although 11 experimental runs were performed, there was no systematic approach for mixing constituents. For the KOSI 3, 4 and 6 experiments, Oehler and Neukum (1991) measured the reflectance spectra at two wavelengths in the visible and in the NIR (0.36 µm and 2.5 µm) before and after the sublimation experiments under three different illumination angles.

Stephens and Gustafson (1991) measured the bidirectional reflectance of ice/carbon, ice/silica and ice/carbon/silica mixtures from the UV to NIR spectral range. But only a single mixing ratio was analysed and the main focus lay on the formation of a surface mantle. The formation and evolution of such mantles from icy samples containing minerals and organic compound was recently investigated by Poch et al. (2016a) and Poch et al. (2016b). It was found that that different mixing types, coatings or inclusions, influence the spectral and morphological evolution of the samples.

The major limitations of previous optical experimental studies to simulate cometary nuclei are the spectral coverage and the sample reproducibility. In the case of Stephens and Gustafson (1991) and Oehler and Neukum (1991) only two wavelengths were analysed. In this work we will show an extensive spectrophotometric study covering the whole VIS-NIR spectral range using six different filter bands to be compared with OSIRIS data. We provide a systematic approach in sample composition as well as in particle sizes, using standardised protocols to ensure reproducibility.

The aim of this study is to see how closely we can match the spectrophotometric properties of 67P described by Fornasier et al. (2015) by combining the three types of materials: carbonaceous compounds (darkening agent), complex organics (spectral reddening agent) and water ice (spectrally neutral agent),

thought to be major constituents of the cometary surface. For each category of material we have selected particularly well characterised samples and mixed them in systematic combinations. The samples were produced with a standardised protocol to reach maximal control on the mixing ratio and the reproducibility. The systematics of such a study are useful for understanding the contributions of individual properties to the global spectrophotometric behaviour.

For all samples the bidirectional reflectance in the VIS-NIR spectral range was measured using the PHIRE-2 goniometer. From these measurements albedos and phase reddening were derived. Complementary results focusing on the surface evolution processes under simulated space conditions will be reported in a follow-up publication.

2. Methods

2.1. Instrument

All measurements presented in this work were acquired using the PHIRE-2 radio-goniometer. Details about the instrument and its calibration can be found in Pommerol et al. (2011) and Jost et al. (2016). Only the relevant specifications are summarised here. The goniometer is located inside a freezer, operated at $-35\,^{\circ}\mathrm{C}$ for ice-bearing samples. Ice-free samples were measured at room temperature. A collimated light source is equipped with six bandpass filters (centred at 450/550/650/750/905/1064 nm) and illuminates the samples with an incidence angle in the range of 0° to 60°. The scattered light is measured with a silicon photovoltaic sensor on another mobile arm, reaching from -80° to $+80^{\circ}$ emission angle. The angle between incidence and emission directions (constant azimuth) is called the phase angle α.

The use of bandpass filters precludes highly resolved spectral data. But since cometary nuclei display featureless spectra in the visible spectral range, without any sharp absorption features, six values in the VIS-NIR range are enough to

PHIRE-2		OSIRIS		
Wavelength (nm)	Bandwidth (nm)	NAC Filter	Wavelength (nm)	Bandwidth (nm)
450±10	70±30	F84	480.7	74.9
550±10	70±30	F83	535.7	62.4
650±10	70±30	F82	649.2	84.5
750±10	70±30	F88	743.7	64.1
905±3.5	25±3.5	F41	882.1	65.9
1064±3.5	25±3.5	F71	989.3	38.2

Table 1: Table listing the PHIRE-2 filters and the corresponding OSIRIS NAC filters with the associated central wavelength and bandwidth.

represent an overall trend in terms of magnitude and slope.

Although the filters used on board OSIRIS are not identical to the ones used in our laboratory study (see Table 1), the results should be qualitatively comparable and we note that our filters have similar or lower bandwidths than the OSIRIS filters.

PHIRE-2 can be equipped with either a mirror head or a beam splitting system (Jost et al., 2016). The advantage of the beamsplitter is the possibility of measuring at very low phase angles (down to 0°) whereas the use of the mirror head results in vignetting of the incident beam for phase angles lower than 4°, preventing any measurement in this configuration. On the other hand, the use of the beamsplitter reduces the signal by a factor 4. Although this is not a problem for bright samples such as those studied by Jost et al. (2016), this causes issues in the case of very dark samples as used in this study. Hence the majority of samples in this study was acquired using the mirror setup.

2.2. Physical units

2.2.1. Reflectance factor

Throughout this manuscript, the measured light is expressed in terms of reflectance factor (REFF) defined as the ratio between the brightness of the sample measured in a particular geometry and the one of a hypothetical Lambertian diffuser (a perfectly diffuse surface which scatters isotropically) observed in the same geometry. The reflectance factor REFF (Hapke, 1993) is related to radiance I [W m^{-2} sr^{-1}] (scattered light) and irradiance F [W/m^2] (incoming light) as $REFF = \pi * I/(F * cos(i))$, where i is the incidence angle of the light source.

2.2.2. Hemispherical albedo (Directional-hemispherical reflectance)

The integrated hemispherical albedo A_H is an import photometric property as it is controlling the energetic budget and therefore the surface temperature. We have thus derived values of A_H by integrating our phase curves over a range of emission angles from 0° to 90° for a vertical illumination. The term $cos(e) \cdot sin(e)$ has the effect that missing values at opposition and at 90° emission angle can be neglected. In case of 2D data (principal plane only) and assuming azimuthal symmetry the hemispherical albedo calculates as follows (see Eq. 10.18 in Hapke (1993)):

$$A_H = 2 \cdot \int_0^{\pi/2} REFF(i, e, a,) \cdot cos(e) \cdot sin(e) de \quad (1)$$

2.3. Phase reddening

Many solar system objects display surface colours that are known to be dependent on the observation geometry. Often, an increase of the spectral slope with increasing solar phase angle is observed in the visible wavelength range. This phenomenon is often referred to as phase reddening. The opposite behaviour, a decrease of the spectral slope with phase angle, is called phase bluing. Reddening is widely observed in our solar system such as e.g. on the

Moon (Gehrels et al., 1964; McCord, 1969) on asteroids (Taylor et al., 1971; Clark et al., 2002; Abe et al., 2006; Magrin et al., 2012) or on comets (Fornasier et al., 2015). Bluing is rarely observed (Rosenbush et al., 2009; Lantz et al., 2015). Schröder et al. (2014) investigated laboratory observations of granular surfaces prepared from different rock types and attempted to reproduce the results by simulation. They showed that microscopic roughness highly influences the spectral slope and its dependence on illumination/measurement geometry.

To be consistent when comparing our results with those of Fornasier et al. (2015); Fornasier et al. (2016), we express the spectral slope in units of % per 100 nm using the same formula (Eq. (2)). Positive values indicate red slopes and negative values blue slopes. At a given phase angle,

$$S[\%/100nm] = \frac{(R_{905} - R_{550})}{R_{550} \times (905nm - 550nm)} \times 10^4 \quad (2)$$

, when the slope S increases as a function of phase angle we call it phase reddening. The 355 nm wide wavelength range over which the spectral slope is calculated is very similar to the one of 347 nm from Fornasier et al. (2015).

2.4. Samples

2.4.1. Ice particle production

For this study we used two types of spherical water ice particles. The "coarse" type has a mean diameter of 67 µm with a standard deviation of 31 µm (as measured by a cryo-SEM), the "fine" type is about ten times smaller with a diameter of 4.54 ± 2.54 µm. For additional details about the production setups and procedures, see Yoldi et al. (2015) and Jost et al. (2016). An overview of all sample materials used in this study is provided in Table 2.

2.4.2. Tholins

We used tholins as analogues of the complex organic matter, because they exhibit a strong red spectral slope from 0.2 to 1.0 µm, allowing us to vary the reddness and albedo of our samples by mixing it with darker and spectrally different carbonaceous compounds. The word "tholins" was first used by Sagan and Khare (1979) to describe the complex macromolecular organics formed after the irradiation of a gas mixture composed of simple molecules, displaying a orange-brownish colour. The yellowish to dark organic residues obtained after the irradiation of simple ices have also been named tholins or "ice tholins" (see e.g. McDonald et al., 1996). The tholins used in this work were previously utilised by Poch et al. (2016a) and Poch et al. (2016b). The material was produced in a plasma of 95 % N_2 and 5 % CH_4, using the PAMPRE setup (Sciamma-O'Brien et al., 2010; Szopa et al., 2006). Tholins are made of a complex mixture of molecular and macromolecular material composed of aliphatic hydrocarbons, nitriles, imines, amines or N-bearing aromatic compounds (Bernard et al., 2006; Carrasco et al., 2009; Pernot et al., 2010; Quirico et al., 2008; Gautier et al., 2014; Gautier et al., 2016). The complex organic molecules are arranged in high porosity spherical grains with a mean diameter of 315 ± 185 nm (Carrasco et al., 2009). Their optical indices have been characterised by Mahjoub et al. (2012) and the reflectance spectra by de Bergh et al. (2008).

2.4.3. Carbon powders

We used carbon powders as analogues of the darkening agent(s) of cometary surfaces. Amorphous carbon inherited from interstellar dust could represent up to 10 % of cometary materials (Wooden, 2008) and could partly contribute to the low albedo of cometary nuclei. However such a high amount of pure carbon in cometary refactory material is questionable, since by date only complex organic materials rather than pure carbons have been found in natural extraterrestrial samples like porous interplanetary dust particles (IDP) or STARDUST samples (e.g. Sandford et al., 2006; Brownlee, 2014).

Carbon black

The carbon black used in this work was purchased from Alfa-Aesar (product 3972). It is the solid residue obtained by acetylene combustion and consists of amorphous carbon shaped as spherical particles with an average diameter of 42 nm. The structure of the individual particles cannot be resolved in Fig. 1a.

Activated charcoal

The activated charcoal used in this study was purchased from Sigma-Aldrich (Product C3345). This granular carbon has been prepared from wood particles which have been impregnated with an unspecified chemical agent and pyrolysed to produce very porous particles of pure carbon. The particles are smaller than 75 µm according to the manufacturer. Our own microscope image analysis resulted in a mean diameter of 17.6 µm with a standard deviation of 11.3 µm. The particle shape is irregular with sharp edges (see Fig. 1b). There is very little formation of agglomerates.

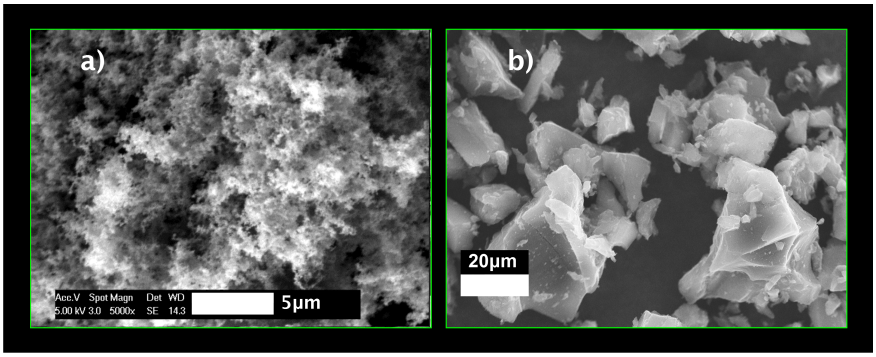

Figure 1: Environmental scanning electron microscope images of of carbon black (a) and activated charcoal (b) acquired at Institute of Geography at University of Bern.

2.5. Mixing types

We developed two different mixing procedures for producing two types of laboratory analogues:

	Particle size	Shape	Bulk density	Porosity
Fine grained ice	4.54 ± 2.54 µm	spherical	$0.11 - 0.19$ g/cm^3	$79 - 88$ %
Coarse grained ice	67 ± 31 µm	spherical	$0.4 - 0.5$ g/cm^3	$46 - 56$ %
Tholins*	315 ± 185 nm	spherical	0.077 ± 0.008 g/cm^3	94.6 ± 0.6 %
Carbon black	42 nm	spherical	$0.08 - 0.12$ g/cm^3	$93 - 95$ %
Activated charcoal	17.6 ± 11.3 µm	spherical	0.31 g/cm^3	81 %

* Brouet et al. (2016)

Table 2: Sample material characteristics

1. Intra-mixture: tholins and carbon particles are mixed in water prior to the freezing process. The non-volatiles are present as inclusions within the icy grains. This mixture type is only applicable for the coarse ice grains. The suspension is prepared by ultrasonication, performed with a Hielscher 200Ht ultrasonic unit equipped with a 7 mm diameter sonotrode. The duration of ultrasonication was limited to about 1 min to keep the suspension temperature below 30 °C, to avoid thermal changes.
2. Inter-mixture: non-volatiles are mixed intimately with the pure water ice particles at the grain level. This process works for both the coarse and the fine particles. The mixture was prepared in an aluminium bottle cooled to liquid nitrogen temperature, by adding freshly produced ice and precooled non-volatiles. The bottle was then agitated using a Vortex-Genie2 mixer at full speed for about 1 min, interrupted for re-cooling the bottle in liquid nitrogen.

The deposition of sample material into the sample holder was done by sieving (800 µm mesh size) to avoid big agglomerates and to produce homogeneous samples of controlled bulk density. There is no compression - the piled material is cut with a spatula and a thin layer of material is sieved on top to obtain a random surface orientation.

3. Laboratory results

In this section we will present experimental results of 3 kinds of mixtures: 1 - carbon-tholin mixtures; 2 - ice-tholin mixtures and 3 - carbon-ice mixtures. The ternary case of ice-carbon-tholin mixtures will be treated in our follow up work.

All datasets shown in this work are publicly available on the Data Analysis Center for Exoplanets (DACE) platform (https://dace.unige.ch/lossy/samplesearch/index) where they can be freely visualized and downloaded.

3.1. Reflectance spectra and albedo

3.1.1. Dry dust mixtures

Despite the fact that carbon black and activated charcoal have the same chemical composition and a similar amorphous structure, their spectral behaviour is different (Fig. 2a). Activated charcoal displays a red spectral slope while carbon black is spectrally blue.

Even with a strong reddening agent, such as tholins, the spectrum remains blue beyond 650 nm, because of the blue spectrum of the nanometre-size carbon black (see Fig. 2b). With such a mixture it is not possible to represent the cometary spectrum, which monotonically increases in the $400 - 1100$ nm range. This could indicate a lower limit to the darkening agent particle size and would exclude particles with a size of a few tens of nanometres, which is consistent with compact particle sizes as observed by GIADA from Fulle et al. (2015) of 30 µm to 1 mm. The detection of "submicron particles" by Della Corte et al. (2015) and Fulle et al. (2015) is quite vague in its definition and not specified in detail.

To reproduce the spectrum of 67P and specifically the red slope, we combined different fractions of tholins from 10 to 50 wt. % with activated charcoal. We

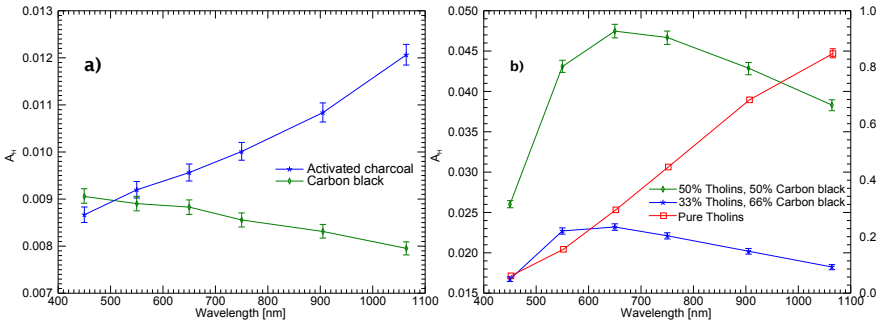

Figure 2: (a) Visible reflectance spectrum of carbon black and activated charcoal. The hemispherical albedo A_H is calculated for each filter band by integration of the phase curve at $i = 0°$. While carbon black with particle sizes smaller than the wavelength has a blue spectral slope, the activated charcoal with particle size much larger than the observed wavelengths has a red slope. (b) Reflectance spectra of carbon black mixed with tholins. Blue, 1:1 mixing ratio, green, 2 wt. parts CB 1 part tholins. The spectrum of pure tholins is overlaid with the y-scale on the right side. The mixture of carbon black (blue slope) with tholins (red slope) results in arch-shaped spectral with a maximum at around 650 nm.

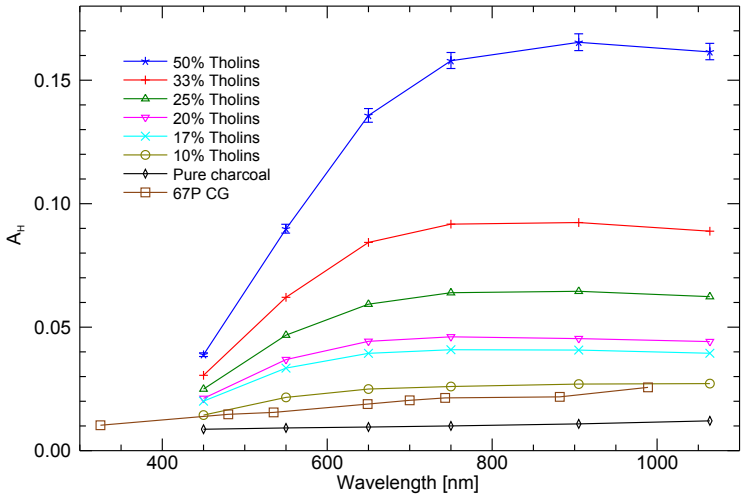

Figure 3: Visible reflectance spectra in units of hemispherical albedo A_H from charcoal mixed with tholins in different ratios. Both constituents have an intrinsic red spectral slope (see Fig. 1). The spectrum of 67P is overplotted. A mixture of charcoal with 10 wt. % of tholins has the highest coincidence with the spectrum of 67P, whereas the slope of the cometary curve is more monotonic increasing. Our mixtures are always concave shaped.

first analysed the mixture as a dry powder without any ice. The values of 67P are calculated by using Hapke parameters fitted to disk-averaged reflectance from Fornasier et al. (2015, Tab. 3). All spectra in Fig. 3 of the charcoal-tholins mixtures show a prominent red slope in the 450 nm to 750 nm range, but are almost flat or even slightly blue towards NIR (where tholins become transparent). The best agreement with the cometary spectrum was reached with a mixture of 90 % charcoal and 10 % tholins. This lab spectrum an the one of the surface of the nucleus intersect at around 450 nm and 1000 nm, but the lab spectrum is less monotonic and displays a concave curvature (being brighter than the cometary surface in the entire $450 - 1000$ nm range).

3.1.2. Ice-tholin mixtures

To study the influence of ice particle size and mixing type on the spectral red slope, we mixed pure water ice with tholins. These mixtures are not representative for comets in terms of brightness. In Fig. 4 as expected a higher tholin content (1 % vs 0.1 %) decreases the albedo in the visible range, but has nearly no effect at 1064 nm (and even already at 905 nm for fine-grained ice). The different mixing type (inter-mixture vs. intra-mixture, see Section 2.5) plays almost no role and differences between the two 0.1 % Tholin samples (with coarse ice grains) may be explained by the very sensitive preparation process, where already minor losses in vessels and tubes can play a significant role. The spectral variations caused by the difference in ice particle size are more prominent. Small ice particles have a higher surface area per unit mass, therefore the relative area coated with tholin particles is smaller, which generally increases the visible albedo. The spectral slopes for coarse and fine-grained ice mixed with 1 % tholins do not differ significantly, despite an offset in albedo of about 0.2 in the VIS range. It is unexpected that at 450 nm and 1064 nm the albedo of pure tholins cannot be distinguished from a mixture of coarse grained ice particles and 1 % tholins.

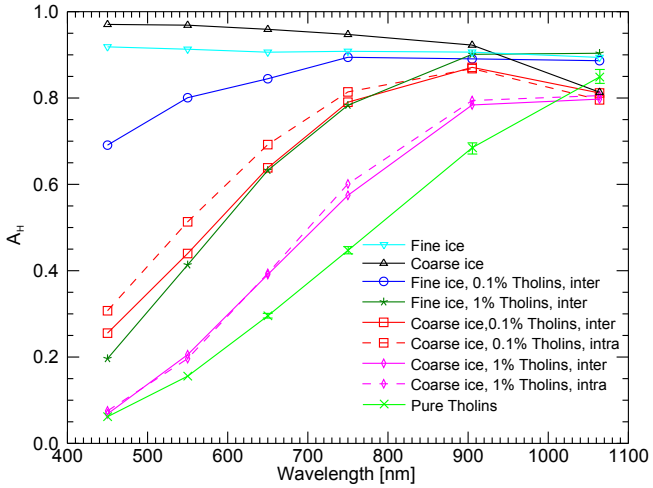

Figure 4: Hemispherical albedo of different ice-tholin mixtures as a function of wavelength. Two different mixing ratios (0.1 and 1 wt. % tholins) were measured. For the coarse grained ice both mixing types (inter + intra mixture; see Section 2.5) were applied. Curves of pure ice and pure tholins are plotted as reference. While at shorter wavelengths (< 750 nm) the tholin content is dominating the albedo, the influence vanishes completely at 1064 nm, where only the ice grain size play a role.

3.1.3. Ice-dust mixtures

To create a dirty-ice mixture with the same albedo as the surface of 67Ps nucleus at a certain wavelength, we analysed all possible combinations of different carbon contaminants and ice particle sizes at different mixing ratios. Their hemispherical albedos are plotted in Fig. 5 as a function of carbon content. The spectral reddening is neglected for this analysis and the wavelength of $\lambda = 750$ nm is selected as it lies in the middle of the analysed spectral range. As a general rule it can be stated that small ice particles need more darkening agent to become dark than coarse ice particles. Smaller carbon particles absorb more efficiently than coarse ones, because the absorbing surface per mass is bigger. In the case of coarse ice particles mixed with nanometre-sized carbon black, only 2 wt. % of contaminant is needed to reach an albedo as low a 67P. In the other extreme case (small ice particles, big charcoal grains) a 1:1 mixing ratio is needed to reach such a low albedo.

To explain the exponential decrease in brightness with contaminant level in Fig. 5, it has to be clarified that both of our mixing types (inter/intra) are intimate mixtures where the two species are mixed as homogeneously as possible at the grain size level. The opposite case is a areal mixture where large chunks of pure material are arranged on the surface (e.g. checkerboard-like). The main difference between these mixing types is the travel-path of a single photon. In an areal mixture each photon ideally "sees" only one species of material until it is scattered or absorbed. The resulting albedo of the total surface is therefore a linear combination of the individual constituents' albedos and their surface covering fraction. A mixture of 50 % charcoal and 50 % ice would result in a hemispherical albedo of ~ 0.5 which is by magnitudes brighter than our laboratory samples. In an intimate mixture, in case of multiple scattering, each photon is very likely to be affected by both constituents within its mean free path length. This effect is most pronounced when the difference in single scattering albedo of the two materials in a binary mixture is large. This reduces

the brightness of an intimate mixture compared to a areal mixture of the same mass ratio. The surface of a cometary nucleus is more likely expected to be an intimate mixture as the grains are small and the primordial mixing took place by condensation and aggregation at small scale level (Greenberg, 1982).

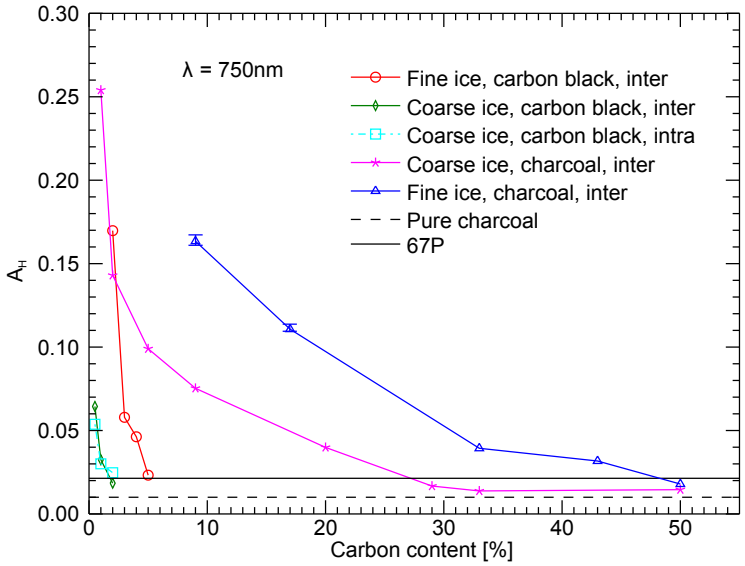

Figure 5: Hemispherical albedo of ice-carbon mixtures as function of carbon content all measured at i = 0° and $\lambda = 750$ nm. Albedos of pure charcoal and 67P are plotted as horizontal reference lines. All possible combinations of ice grains (fine/coarse) and carbon particles (charcoal/carbon black) are shown. Further the combination of coarse ice particles and carbon black was produced using both mixing types (inter/intra mixture), but resulted without noticeable difference in albedo. Generally spoken it can be stated that mixtures of fine grained ice are brighter than with coarse grains when using the same carbon content. Vice versa smaller carbon particles have a bigger darkening effect than bigger ones, when using the mixing ratios. Both findings can be explained by changing total surface area per mass.

3.2. Phase reddening

At larger heliocentric distances ($r_h = 3.6$ AU) in August 2014 the phase reddening effect of 67P was fitted as 0.104 %(100nm)$^{-1}$degree^{-1} (Fornasier et al., 2015) having spectral slopes between 11 and 16 %/100nm at phase angles between 1.3° and 52°. During the period from April to August 2015

($r_h = 1.88 - 1.26$ AU) the phase reddening effect was found to be significantly weaker ($0.041\ \%(100\text{nm})^{-1}\text{degree}^{-1}$; Fornasier et al., 2016) at phase angles between 60° and 90°. This indicates a change in physical properties of the uppermost surface layer (texture and/or composition) during this period.

Comparison of the spectral slopes of carbon-tholin-mixtures, as plotted in Fig. 6, reveal two main trends: whereas the mixtures of carbon-black with tholins show a blue spectral slope ($< 0\%/100$ nm) at low to medium phase angles, they become slightly red at high phase angles ($> 80°$). Mixtures of activated-charcoal with tholins are all red without exceptions, but get redder towards high phase angles.

Varying the mixing ratios mainly results in vertical offsets, the steepness remaining quite constant. Further the steepness of mixtures with carbon black and charcoal seem almost identical. This might be explained by the low absolute spectral slope of carbon materials compared to tholins. The slope is mainly defined by the tholins while the carbon compound/content defines the vertical offset.

A mixture of 33 % tholins and 67 % charcoal could well reproduce the linear fit from Fornasier et al. (2015) with minor discrepancies at phase angles smaller than 20°. While the OSIRIS data indicates an almost linear relationship between phase angle and spectral slope, our measurements show a systematic deviation towards lower values at small phase angle ($\alpha < 15°$). The curve acquired close to perihelion is still best represented by a mixture of 33 % tholins and 67 % charcoal.

To analyse how the carbon content in ice mixtures influences the phase reddening, spectral slopes from mixtures of fine grained ice mixed with charcoal are plotted in Fig. 7a. All curves are fitted by a linear function which is overplotted. Pure fine grained ice displays an almost flat spectrum in the $550 - 950$ nm

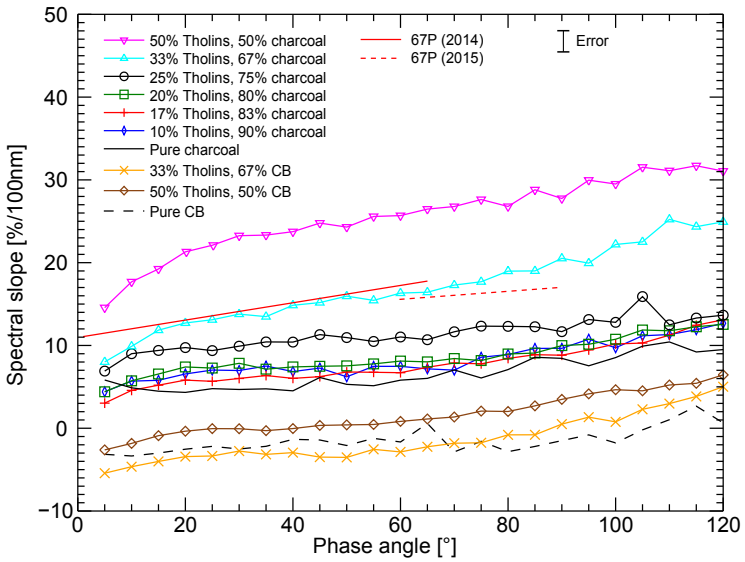

Figure 6: Spectral slopes between 550 nm and 905 nm in units of %/100 nm as a function of phase angle of different carbon–tholin mixtures. All samples were measured at i = 60° to achieve high phase angles. Negative values spectral slope mean a blue spectral slope (i.e. the material is brighter at 550 nm than at 905 nm). All samples show an increasing spectral slope with phase angle. However mixtures using carbon black (see corresponding spectra in Fig. 1) show a negative spectral slope at low phase angle but turn to positive values at high phase angles. Mixtures with the bigger grained charcoal are systematically red at all angular positions. The linear fit of 67P from Fornasier et al. (2015) is represented best by mixture of charcoal with 33 wt. % of tholins.

spectral range and shows nearly no increase of slope with phase angle. Mixtures with charcoal contents from 10 % to 43 % display a slightly blue spectrum (spectral slope <0) at phase angles smaller than 20°, but turn to a red spectrum at larger angles. The 50 % mixture displays a flat spectrum at opposition, then reaches values of about 12 %/100 nm at 120° phase angle. Pure charcoal has a red spectrum at all angles and becomes redder towards high phase angles.

The slopes of the linear fits as a function of charcoal content are plotted in Fig. 7b. There seems to be a correlation between carbon-ice mixing ratio and increase of spectral slope, except for pure charcoal. This seems to be different for charcoal-tholin mixtures (Fig. 6), where the tholin content controls the vertical offset of the curves but not their steepness. This may be a physical effect in mixtures with an almost transparent constituent such as ice, which strongly influences the optical path length.

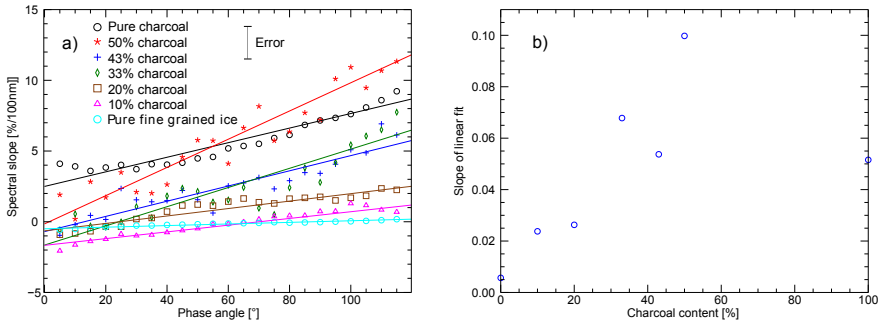

Figure 7: a) Spectral slopes between 550 nm and 905 nm in units of %/100 nm as a function of phase angle for fine grained ice mixed with charcoal. All samples were measured at i = 60°. All curves are fitted by a linear function. Pure ice shows almost no phase reddening, while with higher carbon content the slopes are increasing. The data for pure charcoal do not fit the general trend, the spectrum is redder at low phase angles but the slope lower than for mixtures with 33/43/50 % charcoal. b) The slope of the linear fits as a function of charcoal content, the unit is percent per degree. All charcoal-ice mixtures seem to show a positive correlation of charcoal content and slope.

3.3. Phase curves

In Fig. 8 a variety of different ice-carbon mixtures are compared to the fitted phase curves from 67P at 743 nm (disk integrated) and 649 nm (disk resolved) (Fornasier et al., 2015; Tab 4). OSIRIS data were acquired at phase angles ranging between 1.3° and 54°. Therefore we only compare the curves for phase angles lower than 60°.

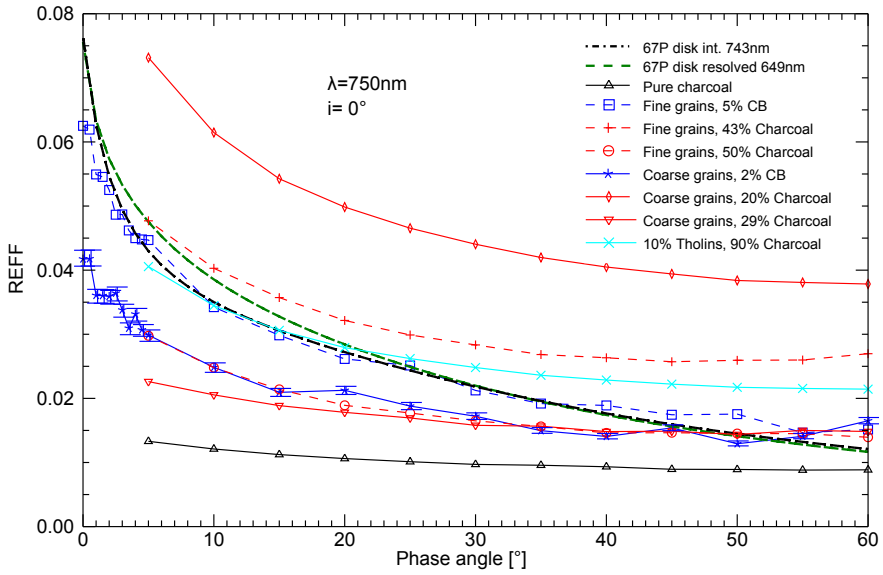

Figure 8: Phase curve of different ice-carbon mixtures acquired at $i = 0°$ and $\lambda = 750$ nm. The curves of fined grained ice with 5 % carbon black and coarse grained ice with 2 % carbon black are measured with the beamsplitter setup (see Section 2.1), the rest with the mirror setup (having a minimal phase angle of 5°). The phase curves of 67P are reproduced from Hapke parameters provided in Fornasier et al. (2015). A mixture fine grained ice mixed with 5 % carbon black matches the cometary phase curves the best in terms of overall reflectance, curvature and opposition peak. Mixtures with coarse grained ice are less convex in general than mixtures with fine grained ice.

First the phase curve of pure activated charcoal is extremely flat and much darker than the cometary phase curve. The mixture of coarse grained ice particles with 29 % charcoal seems to have a nearly constant offset compared to pure charcoal. Coarse ice mixed with 20 % charcoal is by more than factor of

two brighter than 29 % and the phase curve is more curved, especially at phase angles smaller than 25°. The mixture of 2 % carbon black with coarse ice is very similar to the mixture with 29 % charcoal but the slope is steeper at $\alpha < 15°$, indicating a more pronounced opposition peak. A similar behaviour is observed for the mixture of fine grained ice with 50 % charcoal. Fine grained ice with 5 % carbon black shows the most resemblance with the cometary phase curve over all geometries. The maximum amplitude at opposition is clearly lower than on the cometary curve but firstly the minimal phase angle in OSIRIS data is 1.3° and the opposition peak is therefore extrapolated, and secondly our instrument underestimates the amplitude of the peak at exact opposition due to its limited angular resolution (see discussion in Jost et al., 2016). By normalising the phase curves at $\alpha = 5°$ in Fig. 9, absolute differences in reflectance disappear and variations in shape of the phase curves become more visible. The overall darkest samples (pure charcoal and coarse ice with 29 % charcoal) show the flattest phase curves whereas 67P displays the steepest curves. A steep phase curve is usually related to highly porous and/or very rough surfaces where shadowing effects play a bigger role. While large-grained ice particles samples have a bulk density of $0.4 - 0.5$ g/cm^3, fine grained ice samples have bulk densities from 0.11 to 0.19 g/cm^3 and are much more porous.

4. Discussion

After having measured different mixtures of water ice and non-volatile samples, we discuss in this section their different photometric characteristics and set them into the context of the general characteristics of the surface of 67P as well as some local anomalies.

To call two surfaces similar or identical from the point of view of spectrophotometry, different characteristics have to match:

1. The overall brightness/absorptivity, usually expressed by the hemispheric albedo (not influenced by texture)

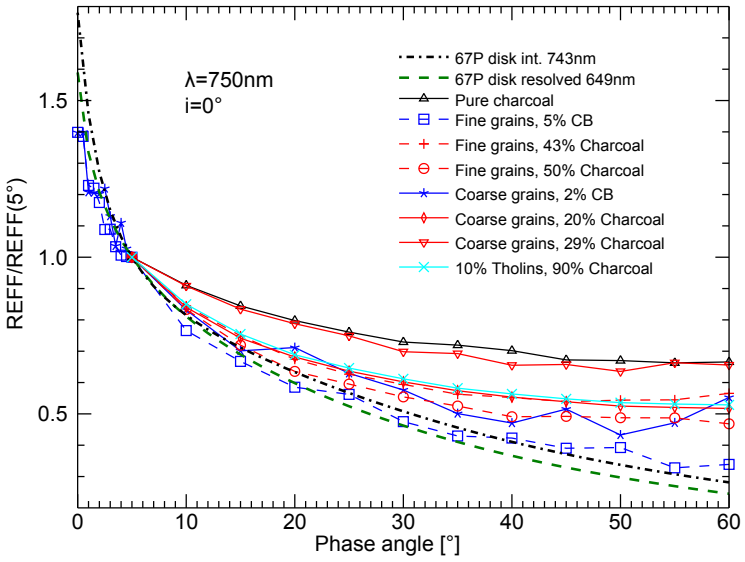

Figure 9: The same phase curves as in Fig. 7 but normalised at $\alpha = 5°$

2. The normal albedo, additionally influenced by the opposition effect (roughness, porosity, grain size)
3. Reflectance spectrum, spectral slope, depth of absorption bands
4. Dependence of the spectrum on the illumination and observation geometries (spectral reddening/bluing)
5. Shape and magnitude of the bidirectional reflectance phase curve
6. Polarisation phase curve (not studied in this work)

To create an ice-bearing two component mixture that matches a given albedo is fairly easy, as long as the darkening agent is darker than the targeted value. But the resulting weight mixing ratio is not unique since the grain sizes of the two materials and the resulting ratio can vary. To infer a darkening agent content from the measured albedo at least a rough estimate of the grain sizes has to be known.

In the case of exposures of metre-sized water ice spots (Pommerol et al., 2015b) which are about ten times brighter (i.e. $A_H \approx 0.2$) than the surround-

ing cometary surface and assuming cometary ice grains in the $33 - 72$ µm range (Filacchione et al., 2016) and individual dust grains smaller than 50 µm (Schulz et al., 2015) we obtain a size ratio $d_{ice}/d_{dust} > 1$. The mixture of fine-grained ice with charcoal in Fig. 4 shows a similar size ratio. An extrapolation of this curve results in a charcoal content of about 5 % to reach an albedo of 0.2, The same ice grains mixed with submicron carbon black particles would need a dust percentage below 1 % to achieve an albedo of 0.2. This is a clear indication that these exposures have to be relatively new and unaltered. To have such low dust content on a metre scale on a cometary surface the bright features are unlikely to be primordial (dust-ice wt. ratio >1) but have to be a result of subsurface recondensation processes, where upstreaming gas from deeper layers is cold trapped below the surface (Filacchione et al., 2016).

The normal albedo is the most difficult parameter to analyse when comparing our laboratory measurements to remote sensing data, since it depends on a single data point (at $\alpha = 0°$) on the phase curve. Hence it is more affected by systematic errors and SNR-limitations that are more prominent when using our zero-phase-angle setup. We underestimate the normal albedo in our lab data by $5 - 10$ % (see discussion in Jost et al., 2016). In addition to the overall brightness of a surface the normal albedo is very sensitive to the contribution of the opposition effect, caused by two different mechanisms. The Shadow Hiding Opposition Effect (SHOE; e.g. Hapke, 1986) is mainly influenced by the macroscopic surface roughness/surface texture, whereas the Coherent Backscattering Opposition Effect (CBOE; e.g. Wolf and Maret, 1985) depends on wavelength, particle size, mean free path (influenced by bulk porosity and packing density) and absorption. Since our cometary analogues are relatively dark, the contribution of CBOE is expected to be low, as shown in Fornasier et al. (2015) and Feller et al. (2016). But this seems not to be generally true for mixtures of bright and dark constituents. In our phase curves (Fig. 6) the porous sample with fine grained ice has significantly higher opposition amplitude than the more compact sample with large-grained ice particles. There is a clear dependence

of porosity and particle size on the opposition peak amplitude which cannot be easily explained by simple shadow hiding mechanisms.

The finding that micrometre-sized activated charcoal displays a red spectral slope while nanometre-sized carbon black is spectrally blue is unexpected but can be explained by different scattering regimes. Such a behaviour is predicted by Mie and Rayleigh theory for spherical particles, as the scattering efficiency Q_s of a particle is dependent on size parameter $x = \pi * D/\lambda$ (and therefore on particle size and wavelength). The maximum efficiency should lay around $x = 5$ (see e.g. Liou, 2002).

There are numerous indications that this effect is not restricted to spherical particles only, as spectral blueing is observed on a variety of dark surfaces throughout the solar system which are not made of spherical particles. Whether Rayleigh scattering is a potential explanation for blue spectral signatures on solar system bodies, such as Saturnian satellites, was discussed in detail recently in Clark et al. (2008), Clark et al. (2012) or Brown (2014). In case of our laboratory sample material activated charcoal with particle sizes of some micrometres has size parameters larger than 100 in the visible spectral range should be in a Mie scattering regime while carbon black with particle size three magnitudes smaller has size parameters below 1 and hence be in a Rayleigh regime. The theoretical size for transition between the two scattering regimes lies between 0.7 µm (at 450 nm) and 1.7 µm (at 1064 nm).

The geometry dependence of the spectral slope (phase reddening/bluing) is still a poorly understood phenomenon. The surfaces of most Solar System objects display an increase of spectral slope with phase angle (reddening, see Section 2.3). This effect needs to be characterised and corrected in order to compare spectra of different surfaces or spectra of a surface acquired at different times and at different phase angle.

By date no physical law predicts a linear phase slope curve and explains the origin of the nonlinear deviation at small phase angles of an almost linear curve in our experimental data. A similar behaviour was found in experimental data (Gradie et al., 1980) and observations of asteroids (Clark et al., 2002). Effects of coherent backscattering mechanisms (Shkuratov et al., 1997; Shkuratov et al., 1999) can be excluded as they mainly act at $\alpha < 2°$, see e.g. Poulet et al. (2002). In Schröder et al. (2014) the role of microscopic and macroscopic surface roughness as a potential cause for monotonic reddening is discussed in detail. Our laboratory samples are all prepared flat on a macroscopic scale while the surface of 67P is not flat at all.

Our measurements reveal that not only the reddening agent (tholins here) has a major influence on the spectral slope but the carbonaceous compound as well. When the carbon particles are small compared to the wavelength (Rayleigh scattering) it is very difficult to achieve a phase reddening similar to the one observed at the surface of 67P. Extreme mixing ratio of $m_{tholins} >> m_{cb}$ would be required to mimic the observations. But in this case the overall magnitude of the spectrum would be far too high (see. Figs. 2 and 3). This sets another constrain on the minimum dust particle size on cometary surfaces of at least a few micrometres.

Further the tholins used in this study are known to be a good analogue of Titan aerosols but not necessarily representative of cometary matter. The analysis of our spectra indicates that the organic material at the surface of 67P nucleus shows a more linear red slope towards the NIR, whereas Titan tholins are almost transparent beyond 1 µm.

While the magnitude of a phase curve is mainly dominated by the albedo of the surface material, its shape depends on surface morphology parameters such as packing density/porosity or macroscopic roughness (boulders, pebbles). The macroscopic roughness does not only affect the reflectance at high phase

angle because of shadowing effects, but it also influences the shape of the opposition surge (see Fig. 8a in Jost et al. (2016)). A rough surface texture usually broadens the SHOE at phase angles up to 20°. At intermediary phase angles the curves become more linear and monotonically decreasing.

In reality the surface roughness is difficult to control and quantify on laboratory samples. In this study all samples have a relatively smooth texture. Samples composed of fine grained ice are rougher because the small ice particles tend to form mm-sized agglomerates.

Another important parameter is the packing density or porosity which is even harder to control than the roughness. There are two potential ways of compacting a granular laboratory sample: a sample is compacted intentionally by adding pressure on the material resulting in a higher bulk density, the second way is a compaction of the top layer while preparing the surface. The second option is much harder to quantify, it is well possible that the uppermost (photometrically relevant) millimetre of a centimetres thick sample is compacted resulting in a vertical packing density gradient, but not showing any noticeable change in bulk density.

The effects of porosity on the surface overall brightness as well as on the phase curves are discussed in Hapke (2008) or Shepard and Helfenstein (2011). In general compact surfaces appear brighter than porous ones, porous surfaces have can have higher reflectance at low phase angles and steeper decreasing phase curves.

In Poch et al. (2016b) it has been demonstrated how a highly porous (> 90 %) sublimation residue of smectite phyllosilicate can change its VIS-NIR spectrum compared to the more compact original state. In the VIS the originally red spectrum became blue, while in the NIR some prominent absorption features vanish. The creation of very porous surfaces as expected in a low gravity environment

on comets is not directly applicable in the lab under ambient pressure conditions.

The nearly perfect match observed between the lab phase curve measured for fine grained ice mixed with 5 % carbon black and the phase curve at the surface of 67P does not mean that the surface on 67P consists of such a mixture. But very pronounced opposition peak on 67P with a high amplitude induces that the uppermost layer (mm to cm) of the comet has to be very porous, since it was impossible to reproduce such a sharp peak using any of our more compact samples. The mixture of 90 % charcoal with 10 % tholins which is the best proxy for the cometary albedo and spectrum has a flatter phase curve with a less pronounced opposition effect. It is very likely that a highly porous matrix of this sample material could mimic the cometary phase curve. Such a structure would be very fragile under terrestrial pressure and gravity regime. Poch et al. (2016a,b) could create such a structure by subliming an ice-bearing mixture of organics and minerals in a thermal vacuum, but it was not possible to transport the sample to the goniometer without damaging the surface residue.

5. Conclusion

By systematic varying input parameters such as grain sizes, water ice content, addition of complex organic compounds and mixing ratios, we were able to produce a laboratory model of the individual global photometric properties such as reflectance spectrum, phase curve, albedo and phase reddening of comet 67P. It was not yet possible to find a laboratory analogue that can provide a match to all cometary surface properties together. This means that at least the composition of our samples is different. Up to now we did not include yet any silicate- or iron-bearing minerals which are known to be present in interplanetary dust.

Our measurements with different carbon compounds support the idea that a lower limit of the mean dust particle size is in the range of some hundreds of nanometres.

Our work demonstrates, in a simple way, that the inversion of a surface composition from remote sensing data in the VIS-NIR spectral range is not straightforward. There are various degrees of freedom such as grain sizes, mixing ratios, physical structure and texture. To achieve a robust match it is vital to constrain at least some of the unknown properties by complementary techniques and instruments.

Acknowledgments

The construction of the facility was funded by the University of Bern and Swiss National Science Foundation (R'equip grant # 206021_133827 and National Centre for Competence in Research *PlanetS*). The authors further thank Stafan Schröder and an anonymus reviewer for helpful suggestions.

References

Abe, M., Takagi, Y., Kitazato, K., Abe, S., Hiroi, T., Vilas, F., Clark, B. E., Abell, P. A., Lederer, S. M., Jarvis, K. S., Nimura, T., Ueda, Y., Fujiwara, A., Jun. 2006. Near-Infrared Spectral Results of Asteroid Itokawa from the Hayabusa Spacecraft. Science 312, 1334–1338.

A'Hearn, M. F., Belton, M. J. S., Delamere, W. A., Feaga, L. M., Hampton, D., Kissel, J., Klaasen, K. P., McFadden, L. A., Meech, K. J., Melosh, H. J., Schultz, P. H., Sunshine, J. M., Thomas, P. C., Veverka, J., Wellnitz, D. D., Yeomans, D. K., Besse, S., Bodewits, D., Bowling, T. J., Carcich, B. T., Collins, S. M., Farnham, T. L., Groussin, O., Hermalyn, B., Kelley, M. S., Kelley, M. S., Li, J.-Y., Lindler, D. J., Lisse, C. M., McLaughlin, S. A., Merlin, F., Protopapa, S., Richardson, J. E., Williams, J. L., Jun. 2011. EPOXI at Comet Hartley 2. Science 332, 1396–1400.

Barucci, M. A., Filacchione, G., Fornasier, S., Raponi, A., Deshapriya, J. D. P., Tosi, F., Feller, C., Ciarniello, M., Sierks, H., Capaccioni, F., Pommerol, A., Massironi, M., Oklay, N., Merlin, F., Vincent, J.-B., Fulchignoni,

M., Guilbert-Lepoutre, A., Perna, D., Capria, M. T., Hasselmann, P. H., Rousseau, B., Barbieri, C., Bockelee-Morvan, D., Lamy, P. L., De Sanctis, C., Rodrigo, R., Erard, S., Koschny, D., Leyrat, C., Rickman, H., Drossart, P., Keller, H. U., A'Hearn, M. F., Arnold, G., Bertaux, J.-L., Bertini, I., Cerroni, P., Cremonese, G., Da Deppo, V., Davidsson, B. J. R., El-Maarry, Fonti, S., Fulle, M., Groussin, O., Guttler, C., Sep. 2016. Detection of exposed H_2O ice on the nucleus of comet 67P/Churyumov-Gerasimenko. ArXiv e-prints.

Bentley, M. S., Torkar, K., Jeszenszky, H., Romstedt, J., Schmied, R., Mannel, T., Oct. 2015. Cometary dust at the nanometre scale - the MIDAS view after perihelion. European Planetary Science Congress 2015, held 27 September - 2 October, 2015 in Nantes, France, Online at http://meetingorganizer.copernicus.org/EPSC2015, id. EPSC2015-441 10, EPSC2015–441.

Bernard, J.-M., Quirico, E., Brissaud, O., Montagnac, G., Reynard, B., McMillan, P., Coll, P., Nguyen, M.-J., Raulin, F., Schmitt, B., Nov. 2006. Reflectance spectra and chemical structure of Titan's tholins: Application to the analysis of Cassini Huygens observations. Icarus 185, 301–307.

Bibring, J.-P., Lamy, P., Langevin, Y., Soufflot, A., Berthé, M., Borg, J., Poulet, F., Mottola, S., Feb. 2007. Civa. Space Science Reviews 128, 397–412.

Brouet, Y., Levasseur-Regourd, A. C., Sabouroux, P., Neves, L., Encrenaz, P., Poch, O., Pommerol, A., Thomas, N., Kofman, W., Le Gall, A., Ciarletti, V., Hérique, A., Lethuillier, A., Carrasco, N., Szopa, C., Nov. 2016. A porosity gradient in 67P/C-G nucleus suggested from CONSERT and SESAME-PP results: an interpretation based on new laboratory permittivity measurements of porous icy analogues. Monthly Notices of the Royal Astronomical Society 462, S89–S98.

Brown, A. J., 2014. Spectral bluing induced by small particles under the mie and rayleigh regimes. Icarus 239, 85 – 95.

Brownlee, D., May 2014. The Stardust Mission: Analyzing Samples from the Edge of the Solar System. Annual Review of Earth and Planetary Sciences 42, 179–205.

Capaccioni, F., Coradini, A., Filacchione, G., Erard, S., Arnold, G., Drossart, P., De Sanctis, M. C., Bockelee-Morvan, D., Capria, M. T., Tosi, F., Leyrat, C., Schmitt, B., Quirico, E., Cerroni, P., Mennella, V., Raponi, A., Ciarniello, M., McCord, T., Moroz, L., Palomba, E., Ammannito, E., Barucci, M. A., Bellucci, G., Benkhoff, J., Bibring, J. P., Blanco, A., Blecka, M., Carlson, R., Carsenty, U., Colangeli, L., Combes, M., Combi, M., Crovisier, J., Encrenaz, T., Federico, C., Fink, U., Fonti, S., Ip, W. H., Irwin, P., Jaumann, R., Kuehrt, E., Langevin, Y., Magni, G., Mottola, S., Orofino, V., Palumbo, P., Piccioni, G., Schade, U., Taylor, F., Tiphene, D., Tozzi, G. P., Beck, P., Biver, N., Bonal, L., Combe, J.-P., Despan, D., Flamini, E., Fornasier, S., Frigeri, A., Grassi, D., Gudipati, M., Longobardo, A., Markus, K., Merlin, F., Orosei, R., Rinaldi, G., Stephan, K., Cartacci, M., Cicchetti, A., Giuppi, S., Hello, Y., Henry, F., Jacquinod, S., Noschese, R., Peter, G., Politi, R., Reess, J. M., Semery, A., Jan. 2015. The organic-rich surface of comet 67P/Churyumov-Gerasimenko as seen by VIRTIS/Rosetta. Science 347 (1), aaa0628.

Carrasco, N., Schmitz-Afonso, I., Bonnet, J.-Y., Quirico, E., Thissen, R., Dutuit, O., Bagag, A., Laprévote, O., Buch, A., Giulani, A., Adandé, G., Ouni, F., Hadamcik, E., Szopa, C., Cernogora, G., Sep. 2009. Chemical Characterization of Titan's Tholins: Solubility, Morphology and Molecular Structure Revisited. Journal of Physical Chemistry A 113, 11195–11203.

Clark, B. E., Helfenstein, P., Bell, J. F., Peterson, C., Veverka, J., Izenberg, N. I., Domingue, D., Wellnitz, D., McFadden, L., Jan. 2002. NEAR Infrared Spectrometer Photometry of Asteroid 433 Eros. Icarus 155, 189–204.

Clark, R. N., Cruikshank, D. P., Jaumann, R., Brown, R. H., Stephan, K., Dalle Ore, C. M., Eric Livo, K., Pearson, N., Curchin, J. M., Hoefen, T. M., Buratti, B. J., Filacchione, G., Baines, K. H., Nicholson, P. D., Apr. 2012.

The surface composition of Iapetus: Mapping results from Cassini VIMS. Icarus 218, 831–860.

Clark, R. N., Curchin, J. M., Jaumann, R., Cruikshank, D. P., Brown, R. H., Hoefen, T. M., Stephan, K., Moore, J. M., Buratti, B. J., Baines, K. H., Nicholson, P. D., Nelson, R. M., 2008. Compositional mapping of saturn's satellite dione with cassini {VIMS} and implications of dark material in the saturn system. Icarus 193 (2), 372 – 386, saturn's Icy Satellites from Cassini.

Colangeli, L., Lopez Moreno, J. J., Palumbo, P., Rodriguez, J., Bussoletti, E., Della Corte, V., Esposito, F., Herranz, M., Jerónimo, J. M., Lopez-Jimenez, A., Epifani, E. M., Morales, R., Palomba, E., Rotundi, A., Vergara, S., International GIADA Team, 2007. GIADA: The Grain Impact Analyser and Dust Accumulator for the Rosetta space mission. Advances in Space Research 39, 446–450.

Coradini, A., Capaccioni, F., Drossart, P., Arnold, G., Ammannito, E., Angrilli, F., Barucci, A., Bellucci, G., Benkhoff, J., Bianchini, G., Bibring, J. P., Blecka, M., Bockelee-Morvan, D., Capria, M. T., Carlson, R., Carsenty, U., Cerroni, P., Colangeli, L., Combes, M., Combi, M., Crovisier, J., De Sanctis, M. C., Encrenaz, E. T., Erard, S., Federico, C., Filacchione, G., Fink, U., Fonti, S., Formisano, V., Ip, W. H., Jaumann, R., Kuehrt, E., Langevin, Y., Magni, G., McCord, T., Mennella, V., Mottola, S., Neukum, G., Palumbo, P., Piccioni, G., Rauer, H., Saggin, B., Schmitt, B., Tiphene, D., Tozzi, G., Feb. 2007. Virtis: An Imaging Spectrometer for the Rosetta Mission. Space Science Reviews 128, 529–559.

de Bergh, C., Schmitt, B., Moroz, L. V., Quirico, E., Cruikshank, D. P., 2008. Laboratory Data on Ices, Refractory Carbonaceous Materials, and Minerals Relevant to Transneptunian Objects and Centaurs. pp. 483–506.

Della Corte, V., Rotundi, A., Fulle, M., Gruen, E., Weissman, P., Sordini, R., Ferrari, M., Ivanovski, S., Lucarelli, F., Accolla, M., Zakharov, V., Mazzotta Epifani, E., Lopez-Moreno, J. J., Rodriguez, J., Colangeli, L., Palumbo, P.,

Bussoletti, E., Crifo, J. F., Esposito, F., Green, S. F., Lamy, P. L., McDonnell, J. A. M., Mennella, V., Molina, A., Morales, R., Moreno, F., Ortiz, J. L., Palomba, E., Perrin, J. M., Rietmeijer, F. J. M., Rodrigo, R., Zarnecki, J. C., Cosi, M., Giovane, F., Gustafson, B., Herranz, M. L., Jeronimo, J. M., Leese, M. R., Lopez-Jimenez, A. C., Altobelli, N., Nov. 2015. GIADA: shining a light on the monitoring of the comet dust production from the nucleus of 67P/Churyumov-Gerasimenko. Astronomy & Astrophysics 583, A13.

Deshapriya, J. D. P., Barucci, M. A., Fornasier, S., Feller, C., Hasselmann, P. H., Sierks, H., El-Maarry, M., Pajola, M., Barbieri, C., Lamy, P. L., Rodrigo, R., Koschny, D., Rickman, H., Agarwal, J., A'Hearn, M. F., Bertaux, J.-L., Bertini, I., Boudreault, S., Cremonese, G., Da Deppo, V., Davidsson, B. J. R., Debei, S., Deller, J., De Cecco, M., Fulle, M., Gicquel, A., Groussin, O., Gutierrez, P. J., Gttler, C., Hofmann, M., Hviid, S. F., Ip, W., Jorda, L., Keller, H. U., Knollenberg, J., Kramm, R., Khrt, E., Kppers, M., Lara, L., Lazzarin, M., Lopez Moreno, J., Marzari, F., Mottola, S., Naletto, G., Oklay, N., Perna, D., Pommerol, A., Thomas, N., Tubiana, C., Vincent, J.-B., 2016. Spectrophotometry of the Khonsu region on the comet 67P/ChuryumovGerasimenko using OSIRIS instrument images. Monthly Notices of the Royal Astronomical Society 462 (Suppl 1), S274–S286.

Feller, C., Fornasier, S., Hasselmann, P. H., Barucci, A., Preusker, F., Scholten, F., Jorda, L., Pommerol, A., Sierks, H., Agarwal, J., A'Hearn, M., Bertaux, J.-L., Bertini, I., Boudreault, S., Cremonese, G., Da Deppo, V., Davidsson, B. J. R., Debei, S., De Cecco, M., Deller, J., Fulle, M., Giquel, A., Groussin, O., Gutierrez, P. J., Güttler, C., Hofmann, M., Hviid, S. F., Keller, H., Ip, W.-H., Knollenberg, J., Kovacs, G., Kramm, J.-R., Kührt, E., Küppers, M., Lara, M. L., Lazzarin, M., Leyrat, C., Lopez Moreno, J. J., Marzari, F., Masoumzadeh, N., Mottola, S., Naletto, G., Oklay, N., Shi, X., Tubiana, C., Vincent, J.-B., 2016. Decimetre-scaled spectrophotometric properties of the nucleus of comet 67p/churyumov–gerasimenko from osiris observations. Monthly Notices of the Royal Astronomical Society 462 (Suppl 1), S287–S303.

Filacchione, G., de Sanctis, M. C., Capaccioni, F., Raponi, A., Tosi, F., Ciarniello, M., Cerroni, P., Piccioni, G., Capria, M. T., Palomba, E., Bellucci, G., Erard, S., Bockelee-Morvan, D., Leyrat, C., Arnold, G., Barucci, M. A., Fulchignoni, M., Schmitt, B., Quirico, E., Jaumann, R., Stephan, K., Longobardo, A., Mennella, V., Migliorini, A., Ammannito, E., Benkhoff, J., Bibring, J. P., Blanco, A., Blecka, M. I., Carlson, R., Carsenty, U., Colangeli, L., Combes, M., Combi, M., Crovisier, J., Drossart, P., Encrenaz, T., Federico, C., Fink, U., Fonti, S., Ip, W. H., Irwin, P., Kuehrt, E., Langevin, Y., Magni, G., McCord, T., Moroz, L., Mottola, S., Orofino, V., Schade, U., Taylor, F., Tiphene, D., Tozzi, G. P., Beck, P., Biver, N., Bonal, L., Combe, J.-P., Despan, D., Flamini, E., Formisano, M., Fornasier, S., Frigeri, A., Grassi, D., Gudipati, M. S., Kappel, D., Mancarella, F., Markus, K., Merlin, F., Orosei, R., Rinaldi, G., Cartacci, M., Cicchetti, A., Giuppi, S., Hello, Y., Henry, F., Jacquinod, S., Reess, J. M., Noschese, R., Politi, R., Peter, G., Jan. 2016. Exposed water ice on the nucleus of comet 67P/Churyumov-Gerasimenko. Nature 529, 368–372.

Fornasier, S., Hasselmann, P. H., Barucci, M. A., Feller, C., Besse, S., Leyrat, C., Lara, L., Gutierrez, P. J., Oklay, N., Tubiana, C., Scholten, F., Sierks, H., Barbieri, C., Lamy, P. L., Rodrigo, R., Koschny, D., Rickman, H., Keller, H. U., Agarwal, J., A'Hearn, M. F., Bertaux, J.-L., Bertini, I., Cremonese, G., Da Deppo, V., Davidsson, B., Debei, S., De Cecco, M., Fulle, M., Groussin, O., Güttler, C., Hviid, S. F., Ip, W., Jorda, L., Knollenberg, J., Kovacs, G., Kramm, R., Kührt, E., Küppers, M., La Forgia, F., Lazzarin, M., Lopez Moreno, J. J., Marzari, F., Matz, K.-D., Michalik, H., Moreno, F., Mottola, S., Naletto, G., Pajola, M., Pommerol, A., Preusker, F., Shi, X., Snodgrass, C., Thomas, N., Vincent, J.-B., Nov. 2015. Spectrophotometric properties of the nucleus of comet 67P/Churyumov-Gerasimenko from the OSIRIS instrument onboard the ROSETTA spacecraft. Astronomy & Astrophysics 583, A30.

Fornasier, S., Mottola, S., Keller, H. U., Barucci, M. A., Davidsson, B., Feller, C., Deshapriya, J. D. P., Sierks, H., Barbieri, C., Lamy, P. L., Rodrigo,

R., Koschny, D., Rickman, H., A'Hearn, M., Agarwal, J., Bertaux, J.-L., Bertini, I., Besse, S., Cremonese, G., Da Deppo, V., Debei, S., De Cecco, M., Deller, J., El-Maarry, M. R., Fulle, M., Groussin, O., Gutierrez, P. J., Güttler, C., Hofmann, M., Hviid, S. F., Ip, W.-H., Jorda, L., Knollenberg, J., Kovacs, G., Kramm, R., Kührt, E., Küppers, M., Lara, M. L., Lazzarin, M., Moreno, J. J. L., Marzari, F., Massironi, M., Naletto, G., Oklay, N., Pajola, M., Pommerol, A., Preusker, F., Scholten, F., Shi, X., Thomas, N., Toth, I., Tubiana, C., Vincent, J.-B., 2016. Rosetta's comet 67p/churyumov-gerasimenko sheds its dusty mantle to reveal its icy nature. Science.

Fulle, M., Della Corte, V., Rotundi, A., Weissman, P., Juhasz, A., Szego, K., Sordini, R., Ferrari, M., Ivanovski, S., Lucarelli, F., Accolla, M., Merouane, S., Zakharov, V., Mazzotta Epifani, E., López-Moreno, J. J., Rodríguez, J., Colangeli, L., Palumbo, P., Grün, E., Hilchenbach, M., Bussoletti, E., Esposito, F., Green, S. F., Lamy, P. L., McDonnell, J. A. M., Mennella, V., Molina, A., Morales, R., Moreno, F., Ortiz, J. L., Palomba, E., Rodrigo, R., Zarnecki, J. C., Cosi, M., Giovane, F., Gustafson, B., Herranz, M. L., Jerónimo, J. M., Leese, M. R., López-Jiménez, A. C., Altobelli, N., Mar. 2015. Density and Charge of Pristine Fluffy Particles from Comet 67P/Churyumov-Gerasimenko. The Astrophysical Journal 802, L12.

Gautier, T., Carrasco, N., Schmitz-Afonso, I., Touboul, D., Szopa, C., Buch, A., Pernot, P., Oct. 2014. Nitrogen incorporation in Titan's tholins inferred by high resolution orbitrap mass spectrometry and gas chromatography-mass spectrometry. Earth and Planetary Science Letters 404, 33–42.

Gautier, T., Schmitz-Afonso, I., Touboul, D., Szopa, C., Buch, A., Carrasco, N., Sep. 2016. Development of HPLC-Orbitrap method for identification of N-bearing molecules in complex organic material relevant to planetary environments. Icarus 275, 259–266.

Gehrels, T., Coffeen, T., Owings, D., Dec. 1964. Wavelength dependance of polarization. III. The lunar surface. Astronomical Journal 69.

Gradie, J., Veverka, J., Buratti, B., 1980. The effects of scattering geometry on the spectrophotometric properties of powdered material. In: Bedini, S. A. (Ed.), Lunar and Planetary Science Conference Proceedings. Vol. 11 of Lunar and Planetary Science Conference Proceedings. pp. 799–815.

Greenberg, J. M., 1982. What are comets made of - A model based on interstellar dust. In: Wilkening, L. L. (Ed.), IAU Colloq. 61: Comet Discoveries, Statistics, and Observational Selection. pp. 131–163.

Gruen, E., Bar-Nun, A., Benkhoff, J., Bischoff, A., Dueren, H., Hellmann, H., Hesselbarth, P., Hsiung, P., Keller, H. U., Klinger, J., 1991. Laboratory simulation of cometary processes - Results from first KOSI experiments. In: Newburn, Jr., R. L., Neugebauer, M., Rahe, J. (Eds.), IAU Colloq. 116: Comets in the post-Halley era. Vol. 167 of Astrophysics and Space Science Library. pp. 277–297.

Gruen, E., Gebhard, J., Bar-Nun, A., Benkhoff, J., Dueren, H., Eich, G., Hische, R., Huebner, W. F., Keller, H. U., Klees, G., Aug. 1993. Development of a dust mantle on the surface of an insolated ice-dust mixture - Results from the KOSI-9 experiment. Journal of Geophysical Research: Planets 98, 15.

Gulkis, S., Frerking, M., Crovisier, J., Beaudin, G., Hartogh, P., Encrenaz, P., Koch, T., Kahn, C., Salinas, Y., Nowicki, R., Irigoyen, R., Janssen, M., Stek, P., Hofstadter, M., Allen, M., Backus, C., Kamp, L., Jarchow, C., Steinmetz, E., Deschamps, A., Krieg, J., Gheudin, M., Bockelée-Morvan, D., Biver, N., Encrenaz, T., Despois, D., Ip, W., Lellouch, E., Mann, I., Muhleman, D., Rauer, H., Schloerb, P., Spilker, T., Feb. 2007. MIRO: Microwave Instrument for Rosetta Orbiter. Space Science Reviews 128, 561–597.

Hapke, B., Aug. 1986. Bidirectional reflectance spectroscopy. 4. - The extinction coefficient and the opposition effect. Icarus 67, 264–280.

Hapke, B., 1993. Theory of reflectance and emittance spectroscopy.

Hapke, B., Jun. 2008. Bidirectional reflectance spectroscopy. 6. Effects of porosity. Icarus 195, 918–926.

Hilchenbach, M., Kissel, J., Langevin, Y., Briois, C., von Hoerner, H., Koch, A., Schulz, R., Siln, J., Altwegg, K., Colangeli, L., Cottin, H., Engrand, C., Fischer, H., Glasmachers, A., Grn, E., Haerendel, G., Henkel, H., Hfner, H., Hornung, K., Jessberger, E. K., Lehto, H., Lehto, K., Raulin, F., Roy, L. L., Ryn, J., Steiger, W., Stephan, T., Thirkell, L., Thomas, R., Torkar, K., Varmuza, K., Wanczek, K.-P., Altobelli, N., Baklouti, D., Bardyn, A., Fray, N., Krger, H., Ligier, N., Lin, Z., Martin, P., Merouane, S., Orthous-Daunay, F. R., Paquette, J., Revillet, C., Siljestrm, S., Stenzel, O., Zaprudin, B., 2016. Comet 67P/ChuryumovGerasimenko: Close-up on Dust Particle Fragments. The Astrophysical Journal Letters 816 (2), L32.

Jost, B., Pommerol, A., Poch, O., Gundlach, B., Leboeuf, M., Dadras, M., Blum, J., Thomas, N., Jan. 2016. Experimental characterization of the opposition surge in fine-grained water-ice and high albedo ice analogs. Icarus 264, 109–131.

Keller, H. U., Barbieri, C., Lamy, P., Rickman, H., Rodrigo, R., Wenzel, K.-P., Sierks, H., A'Hearn, M. F., Angrilli, F., Angulo, M., Bailey, M. E., Barthol, P., Barucci, M. A., Bertaux, J.-L., Bianchini, G., Boit, J.-L., Brown, V., Burns, J. A., Büttner, I., Castro, J. M., Cremonese, G., Curdt, W., da Deppo, V., Debei, S., de Cecco, M., Dohlen, K., Fornasier, S., Fulle, M., Germerott, D., Gliem, F., Guizzo, G. P., Hviid, S. F., Ip, W.-H., Jorda, L., Koschny, D., Kramm, J. R., Kührt, E., Küppers, M., Lara, L. M., Llebaria, A., López, A., López-Jimenez, A., López-Moreno, J., Meller, R., Michalik, H., Michelena, M. D., Müller, R., Naletto, G., Origné, A., Parzianello, G., Pertile, M., Quintana, C., Ragazzoni, R., Ramous, P., Reiche, K.-U., Reina, M., Rodríguez, J., Rousset, G., Sabau, L., Sanz, A., Sivan, J.-P., Stöckner, K., Tabero, J., Telljohann, U., Thomas, N., Timon, V., Tomasch, G., Wittrock, T., Zaccariotto, M., Feb. 2007. OSIRIS - The Scientific Camera System Onboard Rosetta. Space Science Reviews 128, 433–506.

Kissel, J., Altwegg, K., Clark, B. C., Colangeli, L., Cottin, H., Czempiel, S., Eibl, J., Engrand, C., Fehringer, H. M., Feuerbacher, B., Fomenkova, M., Glasmachers, A., Greenberg, J. M., Grün, E., Haerendel, G., Henkel, H., Hilchenbach, M., von Hoerner, H., Höfner, H., Hornung, K., Jessberger, E. K., Koch, A., Krüger, H., Langevin, Y., Parigger, P., Raulin, F., Rüdenauer, F., Rynö, J., Schmid, E. R., Schulz, R., Silén, J., Steiger, W., Stephan, T., Thirkell, L., Thomas, R., Torkar, K., Utterback, N. G., Varmuza, K., Wanczek, K. P., Werther, W., Zscheeg, H., Feb. 2007. Cosima High Resolution Time-of-Flight Secondary Ion Mass Spectrometer for the Analysis of Cometary Dust Particles onboard Rosetta. Space Science Reviews 128, 823–867.

Lantz, C., Brunetto, R., Barucci, M. A., Dartois, E., Duprat, J., Engrand, C., Godard, M., Ledu, D., Quirico, E., May 2015. Ion irradiation of the Murchison meteorite: Visible to mid-infrared spectroscopic results. Astronomy & Astrophysics 577, A41.

Liou, K.-N., 2002. An introduction to atmospheric radiation. Vol. 84. Academic press.

Magrin, S., La Forgia, F., Pajola, M., Lazzarin, M., Massironi, M., Ferri, F., da Deppo, V., Barbieri, C., Sierks, H., Osiris Team, Jun. 2012. (21) Lutetia spectrophotometry from Rosetta-OSIRIS images and comparison to ground-based observations. Planetary and Space Science 66, 43–53.

Mahjoub, A., Carrasco, N., Dahoo, P.-R., Gautier, T., Szopa, C., Cernogora, G., Nov. 2012. Influence of methane concentration on the optical indices of Titan's aerosols analogues. Icarus 221, 670–677.

McCord, T. B., Jun. 1969. Color Differences on the Lunar Surface. Journal of Geophysical Research 74, 3131.

McDonald, G. D., Whited, L. J., DeRuiter, C., Khare, B. N., Patnaik, A., Sagan, C., 1996. Production and chemical analysis of cometary ice tholins. Icarus 122 (1), 107 – 117.

Mottola, S., Arnold, G., Grothues, H.-G., Jaumann, R., Michaelis, H., Neukum, G., Bibring, J.-P., Feb. 2007. The Rolis Experiment on the Rosetta Lander. Space Science Reviews 128, 241–255.

Oehler, A., Neukum, G., Feb. 1991. Visible and near IR albedo measurements of ice/dust mixtures. Geophysical Research Letters 18, 253–256.

Pernot, P., Carrasco, N., Thissen, R., Schmitz-Afonso, I., Jan. 2010. Tholinomics - chemical analysis of nitrogen-rich polymers. Analytical Chemistry 82, 1371–1380.

Poch, O., Pommerol, A., Jost, B., Carrasco, N., Szopa, C., Thomas, N., Mar. 2016a. Sublimation of ice-tholins mixtures: A morphological and spectrophotometric study. Icarus 266, 288–305.

Poch, O., Pommerol, A., Jost, B., Carrasco, N., Szopa, C., Thomas, N., Mar. 2016b. Sublimation of water ice mixed with silicates and tholins: Evolution of surface texture and reflectance spectra, with implications for comets. Icarus 267, 154–173.

Pommerol, A., Thomas, N., Affolter, M., Portyankina, G., Jost, B., Seiferlin, K., Aye, K.-M., Oct. 2011. Photometry and bulk physical properties of Solar System surfaces icy analogs: The Planetary Ice Laboratory at University of Bern. Planetary and Space Science 59, 1601–1612.

Pommerol, A., Thomas, N., El-Maarry, M. R., Pajola, M., Groussin, O., Auger, A.-T., Oklay, N., Fornasier, S., Feller, C., Davidsson, B., Gracia-Berná, A., Jost, B., Marschall, R., Poch, O., Barucci, M. A., Bertaux, J.-L., La Forgia, F., Keller, H. U., Kührt, E., Lowry, S. C., Mottola, S., Naletto, G., Sierks, H., Barbieri, C., Lamy, P. L., Rodrigo, R., Koschny, D., Rickman, H., Agarwal, J., A'Hearn, M. F., Bertini, I., Boudreault, S., Cremonese, G., Da Deppo, V., De Cecco, M., Debei, S., Güttler, C., Fulle, M., Gutierrez, P. J., Hviid, S. F., Ip, W.-H., Jorda, L., Knollenberg, J., Kovacs, G., Kramm, J.-R., Küppers, E., Lara, L., Lazzarin, M., Lopez Moreno, J. L., Marzari,

F., Michalik, H., Preusker, F., Scholten, F., Tubiana, C., Vincent, J.-B., Nov. 2015b. OSIRIS observations of meter-sized exposures of H_2O ice at the surface of 67P/Churyumov-Gerasimenko and interpretation using laboratory experiments. Astronomy & Astrophysics 583, A25.

Poulet, F., Cuzzi, J. N., Cruikshank, D. P., Roush, T., Dalle Ore, C. M., Dec. 2002. Comparison between the Shkuratov and Hapke Scattering Theories for Solid Planetary Surfaces: Application to the Surface Composition of Two Centaurs. Icarus 160, 313–324.

Protopapa, S., Sunshine, J. M., Feaga, L. M., Kelley, M. S. P., A'Hearn, M. F., Farnham, T. L., Groussin, O., Besse, S., Merlin, F., Li, J.-Y., Aug. 2014. Water ice and dust in the innermost coma of comet 103P/Hartley 2. Icarus 238, 191–204.

Quirico, E., Montagnac, G., Lees, V., McMillan, P. F., Szopa, C., Cernogora, G., Rouzaud, J.-N., Simon, P., Bernard, J.-M., Coll, P., Fray, N., Minard, R. D., Raulin, F., Reynard, B., Schmitt, B., Nov. 2008. New experimental constraints on the composition and structure of tholins. Icarus 198, 218–231.

Riedler, W., Torkar, K., Jeszenszky, H., Romstedt, J., Alleyne, H. S. C., Arends, H., Barth, W., Biezen, J. V. D., Butler, B., Ehrenfreund, P., Fehringer, M., Fremuth, G., Gavira, J., Havnes, O., Jessberger, E. K., Kassing, R., Klöck, W., Koeberl, C., Levasseur-Regourd, A. C., Maurette, M., Rüdenauer, F., Schmidt, R., Stangl, G., Steller, M., Weber, I., Feb. 2007. MIDAS The Micro-Imaging Dust Analysis System for the Rosetta Mission. Space Science Reviews 128, 869–904.

Rosenbush, V. K., Shevchenko, V. G., Kiselev, N. N., Sergeev, A. V., Shakhovskoy, N. M., Velichko, F. P., Kolesnikov, S. V., Karpov, N. V., Jun. 2009. Polarization and brightness opposition effects for the E-type Asteroid 44 Nysa. Icarus 201, 655–665.

Sagan, C., Khare, B. N., Jan. 1979. Tholins - Organic chemistry of interstellar grains and gas. Nature 277, 102–107.

Sandford, S. A., Aléon, J., Alexander, C. M. O. ., Araki, T., Bajt, S., Baratta, G. A., Borg, J., Bradley, J. P., Brownlee, D. E., Brucato, J. R., Burchell, M. J., Busemann, H., Butterworth, A., Clemett, S. J., Cody, G., Colangeli, L., Cooper, G., D'Hendecourt, L., Djouadi, Z., Dworkin, J. P., Ferrini, G., Fleckenstein, H., Flynn, G. J., Franchi, I. A., Fries, M., Gilles, M. K., Glavin, D. P., Gounelle, M., Grossemy, F., Jacobsen, C., Keller, L. P., Kilcoyne, A. L. D., Leitner, J., Matrajt, G., Meibom, A., Mennella, V., Mostefaoui, S., Nittler, L. R., Palumbo, M. E., Papanastassiou, D. A., Robert, F., Rotundi, A., Snead, C. J., Spencer, M. K., Stadermann, F. J., Steele, A., Stephan, T., Tsou, P., Tyliszczak, T., Westphal, A. J., Wirick, S., Wopenka, B., Yabuta, H., Zare, R. N., Zolensky, M. E., Dec. 2006. Organics Captured from Comet 81P/Wild 2 by the Stardust Spacecraft. Science 314, 1720.

Schröder, S. E., Grynko, Y., Pommerol, A., Keller, H. U., Thomas, N., Roush, T. L., Sep. 2014. Laboratory observations and simulations of phase reddening. Icarus 239, 201–216.

Schröder, S. E., Mottola, S., Arnold, G., Grothues, H.-G., Jaumann, R., Keller, H. U., Michaelis, H., Bibring, J.-P., Pelivan, I., Koncz, A., Otto, K., Remetean, E., Souvannavong, F., Dolives, B., Mar. 2017. Close-up images of the final Philae landing site on comet 67P/Churyumov-Gerasimenko acquired by the ROLIS camera. Icarus 285, 263–274.

Schulz, R., Hilchenbach, M., Langevin, Y., Kissel, J., Silen, J., Briois, C., Engrand, C., Hornung, K., Baklouti, D., Bardyn, A., Cottin, H., Fischer, H., Fray, N., Godard, M., Lehto, H., Le Roy, L., Merouane, S., Orthous-Daunay, F.-R., Paquette, J., Rynö, J., Siljeström, S., Stenzel, O., Thirkell, L., Varmuza, K., Zaprudin, B., Feb. 2015. Comet 67P/Churyumov-Gerasimenko sheds dust coat accumulated over the past four years. Nature 518, 216–218.

Sciamma-O'Brien, E., Carrasco, N., Szopa, C., Buch, A., Cernogora, G., 2010. Titan's atmosphere: an optimal gas mixture for aerosol production? Icarus 209 (2), 704–714.

Sears, D. W. G., Kochan, H. W., Huebner, W. F., 1999. Laboratory simulation of the physical processes occurring on and near the surfaces of comet nuclei. Meteoritics & Planetary Science 34 (4), 497–525.

Seiferlin, K., Spohn, T., Benkhoff, J., Jul. 1995. Cometary ice texture and the thermal evolution of comets. Advances in Space Research 15, 35–38.

Shepard, M. K., Helfenstein, P., 2011. A laboratory study of the bidirectional reflectance from particulate samples. Icarus 215 (2), 526 – 533.

Shkuratov, Y., Starukhina, L., Hoffmann, H., Arnold, G., Feb. 1999. A Model of Spectral Albedo of Particulate Surfaces: Implications for Optical Properties of the Moon. Icarus 137, 235–246.

Shkuratov, Y. G., Stankevich, D. G., Ovcharenko, A. A., Korokhin, V. V., 1997. A Study of Light Backscattering from Planetary-Regolith-Type Surfaces at Phase Angles 0.2deg-3.5deg. Solar System Research 31, 50.

Sierks, H., Barbieri, C., Lamy, P. L., Rodrigo, R., Koschny, D., Rickman, H., Keller, H. U., Agarwal, J., A'Hearn, M. F., Angrilli, F., Auger, A.-T., Barucci, M. A., Bertaux, J.-L., Bertini, I., Besse, S., Bodewits, D., Capanna, C., Cremonese, G., Da Deppo, V., Davidsson, B., Debei, S., De Cecco, M., Ferri, F., Fornasier, S., Fulle, M., Gaskell, R., Giacomini, L., Groussin, O., Gutierrez-Marques, P., Gutiérrez, P. J., Güttler, C., Hoekzema, N., Hviid, S. F., Ip, W.-H., Jorda, L., Knollenberg, J., Kovacs, G., Kramm, J. R., Kührt, E., Küppers, M., La Forgia, F., Lara, L. M., Lazzarin, M., Leyrat, C., Lopez Moreno, J. J., Magrin, S., Marchi, S., Marzari, F., Massironi, M., Michalik, H., Moissl, R., Mottola, S., Naletto, G., Oklay, N., Pajola, M., Pertile, M., Preusker, F., Sabau, L., Scholten, F., Snodgrass, C., Thomas, N., Tubiana, C., Vincent, J.-B., Wenzel, K.-P., Zaccariotto, M., Pätzold, M., Jan. 2015. On the nucleus structure and activity of comet 67P/Churyumov-Gerasimenko. Science 347 (1), aaa1044.

Stephens, J. R., Gustafson, B. A. S., Nov. 1991. Laboratory reflectance mea-

surements of analogues to 'dirty' ice surfaces on atmosphereless solar system bodies. Icarus 94, 209–217.

Sunshine, J. M., A'Hearn, M. F., Groussin, O., Li, J.-Y., Belton, M. J. S., Delamere, W. A., Kissel, J., Klaasen, K. P., McFadden, L. A., Meech, K. J., Melosh, H. J., Schultz, P. H., Thomas, P. C., Veverka, J., Yeomans, D. K., Busko, I. C., Desnoyer, M., Farnham, T. L., Feaga, L. M., Hampton, D. L., Lindler, D. J., Lisse, C. M., Wellnitz, D. D., Mar. 2006. Exposed Water Ice Deposits on the Surface of Comet 9P/Tempel 1. Science 311, 1453–1455.

Sunshine, J. M., Feaga, L. M., Groussin, O., Besse, S., Protopapa, S., Merlin, F., Farnham, T. L., A'Hearn, M. F., Dixi Science Team, Mar. 2011. Icy Grains in Comet 103P/Hartley 2. In: Lunar and Planetary Science Conference. Vol. 42 of Lunar and Planetary Science Conference. p. 2292.

Szopa, C., Cernogora, G., Boufendi, L., Correia, J. J., Coll, P., Apr. 2006. PAMPRE: A dusty plasma experiment for Titan's tholins production and study. Planetary and Space Science 54, 394–404.

Taylor, R. C., Gehrels, T., Silvester, A. B., Mar. 1971. Minor Planets and Related Objects. VI. Asteroid (110) Lydia. Astronomical Journal 76, 141.

Thomas, N., Sierks, H., Barbieri, C., Lamy, P. L., Rodrigo, R., Rickman, H., Koschny, D., Keller, H. U., Agarwal, J., A'Hearn, M. F., Angrilli, F., Auger, A.-T., Barucci, M. A., Bertaux, J.-L., Bertini, I., Besse, S., Bodewits, D., Cremonese, G., Da Deppo, V., Davidsson, B., De Cecco, M., Debei, S., El-Maarry, M. R., Ferri, F., Fornasier, S., Fulle, M., Giacomini, L., Groussin, O., Gutierrez, P. J., Güttler, C., Hviid, S. F., Ip, W.-H., Jorda, L., Knollenberg, J., Kramm, J.-R., Kührt, E., Küppers, M., La Forgia, F., Lara, L. M., Lazzarin, M., Moreno, J. J. L., Magrin, S., Marchi, S., Marzari, F., Massironi, M., Michalik, H., Moissl, R., Mottola, S., Naletto, G., Oklay, N., Pajola, M., Pommerol, A., Preusker, F., Sabau, L., Scholten, F., Snodgrass, C., Tubiana, C., Vincent, J.-B., Wenzel, K.-P., Jan. 2015. The morphological diversity of comet 67P/Churyumov-Gerasimenko. Science 347 (1), aaa0440.

Wolf, P.-E., Maret, G., Dec 1985. Weak Localization and Coherent Backscattering of Photons in Disordered Media. Physical Review Letters 55, 2696–2699.

Wooden, D. H., 2008. Cometary Refractory Grains: Interstellar and Nebular Sources. Springer New York, New York, NY, pp. 75–108.

Yoldi, Z., Pommerol, A., Jost, B., Poch, O., Gouman, J., Thomas, N., Aug. 2015. VIS-NIR reflectance of water ice/regolith analogue mixtures and implications for the detectability of ice mixed within planetary regoliths. Geophysical Research Letters 42, 6205–6212.